

Femtosecond spectral interferometry of optical activity: Theory

Hanju Rhee,¹ Jeong-Hyon Ha,² Seung-Joon Jeon,^{1,2} and Minhaeng Cho^{1,2,a)}

¹Department of Chemistry and Center for Multidimensional Spectroscopy, Korea University, Seoul 136-701, Republic of Korea

²Multidimensional Spectroscopy Laboratory, Korea Basic Science Institute, Seoul 136-713, Republic of Korea

(Received 27 March 2008; accepted 15 July 2008; published online 4 September 2008)

Optical activities such as circular dichroism (CD) and optical rotatory dispersion (ORD) are manifested by almost all natural products. However, the CD is an extremely weak effect so that time-resolved CD spectroscopy has been found to be experimentally difficult and even impossible for vibrational CD with current technology. Here, we show that the weak-signal and nonzero background problems can be overcome by heterodyned spectral interferometric detection of the phase and amplitude of optical activity free-induction-decay (OA FID) field. A detailed theoretical description and a cross-polarization scheme for selectively measuring the OA FID are presented and discussed. It is shown that the parallel and perpendicular electric fields when the solution sample contains chiral molecules are coupled to each other. Therefore, simultaneous spectral interferometric measurements of the parallel and perpendicular FID fields can provide the complex susceptibility, which is associated with the circular dichroism and optical rotatory dispersion as its imaginary and real parts, respectively. On the basis of the theoretical results, to examine its experimental possibility, we present numerical simulations for a model system. We anticipate the method discussed here to be a valuable tool for detecting electronic or vibrational optical activity in femtosecond time scale. © 2008 American Institute of Physics. [DOI: 10.1063/1.2968130]

I. INTRODUCTION

Circular dichroism (CD) spectroscopy is to measure the differential absorption coefficients of chiral molecules when the incident radiation is left- and right-circularly polarized (LCP and RCP).¹ The electronic and vibrational CD (VCD) spectroscopy has been applied to a wide range of chemical and biological systems in condensed phases, and particularly it has been shown to be an incisive tool to determine the secondary structure of polypeptide in a thermal equilibrium state.¹ However, to study dynamical evolution of biomolecules when they are participated in biological reactions or undergo conformational transitions, it has been necessary to develop time-resolved CD spectroscopic techniques. In this regard, there have been a number of efforts to shorten the time scale achievable by thus developed time-resolved CD spectrometer.^{2–8} In the case of electronic CD, it was shown that nanosecond CD measurement can be achieved by detecting the difference between the left-elliptically polarized (LEP) and right-elliptically polarized (REP) beam interactions with chiral molecular solution^{2–4,9} or by measuring the optical rotatory dispersion (ORD) spectrum with a quasinull geometry.^{10–12} Note that the ORD spectrum is in principle related to the CD spectrum via the Kramers–Kronig transformation.¹ Alternative approaches were also accomplished by combining an ultrashort laser with an electro-optic modulator or a Babinet–Soleil compensator to measure picosecond electronic CD or ORD.^{13,14} Xie and Simon¹³

have developed a picosecond time-resolved CD spectrometer employing a picosecond dye laser and a Pockels' cell and observed ultrafast dynamics occurring in the tertiary structure of (carbon monoxy)myoglobin after the photodissociation of CO.⁶

Often, certain chemical and biochemical reactions involve ultrafast structural or conformational changes in time scale ranging from femtosecond to subnanosecond, e.g., enzyme catalysis, early parts of protein folding and unfolding, chemical reaction dynamics involving chiral reactants or products, etc. To enable us to follow the chirality changes of these reactive systems in time, one might need an ultrafast CD spectroscopy that operates in subpicosecond time scale. However, conventional time-resolved CD is based on the differential measurement technique, i.e., $\Delta A = A_{LCP} - A_{RCP}$ or $\Delta A = A_{LEP} - A_{REP}$. Consequently, it has been quite difficult to discriminate miniscule CD signals from the large achiral background signal. Here, we theoretically show that the optical activity free induction decay (OA FID) measurement can be possible if its detection is performed by using the heterodyned spectral interferometric detection^{15–30} scheme. Recently, Abramavicius and Mukamel^{31,32} theoretically showed that the nonlinear optical activity can be studied by considering the polarization beyond the electric dipole approximation. Note that the spectral interferometry has been known to be extremely useful for measuring very weak-signal field in the frequency domain by using a multichannel array detector.^{15,17–22,24,25,33} Instead of time-domain interference measurement technique, the spectral interferometry has been found to be exceptionally useful in quantitatively determining both the amplitude and the phase of the weak-signal

^{a)}Author to whom correspondence should be addressed: Electronic mail: mcho@korea.ac.kr.

field.^{19,21} We demonstrate that a particular choice of polarization directions of the incident beam and detected FID field enables one to selectively measure the OA FID signal field so that the weak-signal and large background problems of the conventional CD measurement technique can be overcome by the technique theoretically proposed here. In addition, numerical simulation results will be presented to examine the experimental possibility of spectral interferometric detection of the OA FID signal field in femtosecond time scale.

II. LINEAR RESPONSE THEORY

From the minimal coupling Hamiltonian, the radiation-molecule interaction energy is³⁴

$$H_I = -\frac{e}{mc}\mathbf{A}(\mathbf{r},t) \cdot \mathbf{p}, \quad (1)$$

where \mathbf{A} is the vector potential and \mathbf{p} is the quantum mechanical momentum operator. The vector potential is assumed to be given as

$$\mathbf{A}(\mathbf{r},t) = \epsilon A_0 f(t) \cos(\mathbf{k} \cdot \mathbf{r} - \omega_c t), \quad (2)$$

where ϵ is the unit vector, A_0 the amplitude, $f(t)$ the temporal envelop function that is real, \mathbf{k} the wavevector, and ω_c the center frequency. Combining Eqs. (1) and (2), one can rewrite the interaction Hamiltonian as

$$H_I = -U(\mathbf{k})F(t) - U(-\mathbf{k})F^*(t), \quad (3)$$

with

$$U(\mathbf{k}) = \frac{eA_0}{2mc} e^{i\mathbf{k} \cdot \mathbf{r}} (\epsilon \cdot \mathbf{p}) = \frac{eA_0}{2mc} (\epsilon \cdot \mathbf{p}) + \frac{ieA_0}{2mc} (\mathbf{k} \cdot \mathbf{r}) (\epsilon \cdot \mathbf{p}) + \dots$$

$$F(t) = f(t) e^{-i\omega_c t}. \quad (4)$$

The first and second terms in Eq. (3) are known to cause absorption and stimulated emission, respectively. Since we will consider an absorption process of a molecule in the ground state, it is sufficient to take into consideration of the first term in Eq. (3).

It is assumed that there is no equilibrium dipole moment of the solution sample and that the solution sample is translationally invariant and time stationary. Then, from the linear response theory,³⁵ the average dipole $\langle \boldsymbol{\mu}(t) \rangle$ is given as

$$\langle \boldsymbol{\mu}(t) \rangle = \int_0^t d\tau \boldsymbol{\varphi}(t-\tau) F(\tau), \quad (5)$$

where the vectorial linear response (or after effect) function is defined as

$$\boldsymbol{\varphi}(t) = \frac{i}{\hbar} \langle [\boldsymbol{\mu}(t), U(\mathbf{k})] \rho \rangle. \quad (6)$$

Here the time evolution of the operator is described in the Heisenberg representation, e.g., $\boldsymbol{\mu}(t) = e^{-iH_0 t/\hbar} \boldsymbol{\mu} e^{-iH_0 t/\hbar}$ and $U(\mathbf{k})$ is the operator at time zero. ρ is the canonical density operator given as a product of system and bath terms as $\rho = \rho_S \rho_B$. From the definition of the macroscopic polarization $\mathbf{P}(t)$, we have

$$\mathbf{P}(t) = \frac{N}{V} \langle \boldsymbol{\mu}(t) \rangle = \frac{N}{V} \int_0^t d\tau \boldsymbol{\varphi}(t-\tau) F(\tau), \quad (7)$$

where N and V are the number of molecules and volume, respectively. Inserting $U(\mathbf{k})$ in Eq. (4) into Eq. (6) and considering the first two terms in the series expansion of $U(\mathbf{k})$ with respect to \mathbf{k} , one can obtain the linear response function as

$$\boldsymbol{\varphi}(t) = \frac{eA_0}{2mc} \left(\frac{i}{\hbar} \right) \{ \boldsymbol{\psi}_0(t) + \boldsymbol{\psi}_1(t) \}, \quad (8)$$

where

$$\boldsymbol{\psi}_0(t) = \langle [\boldsymbol{\mu}(t), \epsilon \cdot \mathbf{p}(0)] \rho \rangle, \quad (9)$$

$$\boldsymbol{\psi}_1(t) = \langle [\boldsymbol{\mu}(t), i(\mathbf{k} \cdot \mathbf{r}(0)) (\epsilon \cdot \mathbf{p}(0))] \rho \rangle. \quad (10)$$

Now, using the relationship between \mathbf{p} and \mathbf{r} operators, $\mathbf{p} = (im/\hbar)[H_0, \mathbf{r}]$, and assuming that the ground state is only populated at room temperature, i.e., $\rho_S = |g\rangle\langle g|$, we find that $\boldsymbol{\psi}_0(t)$ is given as

$$\boldsymbol{\psi}_0(t) = \frac{im}{e} \sum_e \omega_{eg} \{ \langle \boldsymbol{\mu}_{ge}(t) (\epsilon \cdot \boldsymbol{\mu}_{eg}(0)) \rho_B \rangle_B + \langle (\epsilon \cdot \boldsymbol{\mu}_{ge}(0)) \boldsymbol{\mu}_{eg}(t) \rho_B \rangle_B \}, \quad (11)$$

where $\boldsymbol{\mu}_{ge}(t) = \langle g | \boldsymbol{\mu}(t) | e \rangle$ and $\omega_{eg} = (E_e - E_g)/\hbar$. In Eq. (11), $\langle \dots \rangle_B$ is the trace operation over the bath eigenstates. It should be noted that $\boldsymbol{\mu}_{ge}(t)$ is highly oscillating and approximately proportional to $\exp(-i\omega_{eg}t)$. In a resonant condition, ω_{eg} in the first (second) term of Eq. (11) can be replaced with ω_c ($-\omega_c$). Therefore, we have

$$\boldsymbol{\psi}_0(t) = \frac{im\omega_c}{e} \langle [\boldsymbol{\mu}(t), (\epsilon \cdot \boldsymbol{\mu}(0))] \rho \rangle. \quad (12)$$

Note that thus obtained $\boldsymbol{\psi}_0(t)$ in Eq. (12) differs from the usual dipole-dipole impulsive response function by a constant factor.

We next consider the second term $\boldsymbol{\psi}_1(t)$ in Eq. (8). Using the property of cross product, one can rewrite $\boldsymbol{\psi}_1(t)$ as a sum of two terms, i.e.,

$$\boldsymbol{\psi}_1(t) = \boldsymbol{\psi}_M(t) + \boldsymbol{\psi}_Q(t), \quad (13)$$

where $\boldsymbol{\psi}_M(t)$ and $\boldsymbol{\psi}_Q(t)$ are the electric dipole-magnetic dipole term and the electric dipole-electric quadrupole term, respectively, and they are given as

$$\boldsymbol{\psi}_M(t) = \frac{i}{2} \langle [\boldsymbol{\mu}(t), (\mathbf{k} \times \epsilon) \cdot (\mathbf{r}(0) \times \mathbf{p}(0))] \rho \rangle, \quad (14)$$

$$\boldsymbol{\psi}_Q(t) = \frac{i}{2} \langle [\boldsymbol{\mu}(t), (\mathbf{k} \cdot \mathbf{r}(0)) (\epsilon \cdot \mathbf{p}(0)) + (\epsilon \cdot \mathbf{r}(0)) \times (\mathbf{k} \cdot \mathbf{p}(0))] \rho \rangle. \quad (15)$$

Since the magnetic dipole operator is defined as $\mathbf{M} = (e/2mc)\mathbf{L} = (e/2mc)\mathbf{r} \times \mathbf{p}$, Eq. (14) can be rewritten as

$$\psi_M(t) = \frac{imc}{e} \langle [\boldsymbol{\mu}(t), (\mathbf{k} \times \boldsymbol{\varepsilon}) \cdot \mathbf{M}(0)] \rangle \rho. \quad (16)$$

From the definition of electric quadrupole operator $\mathbf{Q} = e^2 \sum_{ij} \mathbf{r}_i \mathbf{r}_j$ and using the following operator identity, $\mathbf{p} = (im/\hbar)[H_0, \mathbf{r}]$, we find that the electric dipole–electric quadrupole response function is

$$\psi_Q(t) = -\frac{m\omega_c}{2e^2} \langle [\boldsymbol{\mu}(t), \boldsymbol{\varepsilon} \cdot \mathbf{Q}(0) \cdot \mathbf{k}] \rangle \rho. \quad (17)$$

Combining all three contributions to $\varphi(t)$, which were given in Eqs. (12), (16), and (17), we find that the linear response function is, in general, given as

$$\begin{aligned} \varphi(t) = & \frac{iA_0\omega_c}{2c} \left(\frac{i}{\hbar} \right) \langle [\boldsymbol{\mu}(t), (\boldsymbol{\varepsilon} \cdot \boldsymbol{\mu}(0))] \rangle \rho \\ & + \frac{iA_0}{2} \left(\frac{i}{\hbar} \right) \langle [\boldsymbol{\mu}(t), (\mathbf{k} \times \boldsymbol{\varepsilon}) \cdot \mathbf{M}(0)] \rangle \rho \\ & - \frac{A_0\omega_c}{4ec} \left(\frac{i}{\hbar} \right) \langle [\boldsymbol{\mu}(t), \boldsymbol{\varepsilon} \cdot \mathbf{Q}(0) \cdot \mathbf{k}] \rangle \rho. \end{aligned} \quad (18)$$

The second term represents the molecular response when the molecular magnetic dipole interacts with the magnetic field of the incident beam. The third term describes the response to the electric quadrupole–electric field interaction. The results above are, however, not complete yet because the macroscopic polarization includes additional contributions from magnetic dipole and electric quadrupole terms that are $\langle \mathbf{M}(t) \rangle \times \hat{\mathbf{k}}$ and $(i/2)\mathbf{k} \cdot \langle \mathbf{Q}(t) \rangle$. By including the lowest order contributions to the linear polarization, the response function in Eq. (18') is found to be

$$\begin{aligned} \varphi(t) = & \frac{iA_0\omega_c}{2c} \left(\frac{i}{\hbar} \right) \langle [\boldsymbol{\mu}(t), (\boldsymbol{\varepsilon} \cdot \boldsymbol{\mu}(0))] \rangle \rho \\ & + \frac{iA_0}{2} \left(\frac{i}{\hbar} \right) \langle [\boldsymbol{\mu}(t), (\mathbf{k} \times \boldsymbol{\varepsilon}) \cdot \mathbf{M}(0)] \rangle \rho \\ & - \frac{A_0\omega_c}{4ec} \left(\frac{i}{\hbar} \right) \langle [\boldsymbol{\mu}(t), \boldsymbol{\varepsilon} \cdot \mathbf{Q}(0) \cdot \mathbf{k}] \rangle \rho \\ & + \frac{iA_0}{2} \left(\frac{i}{\hbar} \right) \langle [\mathbf{M}(t) \times \mathbf{k}, \boldsymbol{\varepsilon} \cdot \boldsymbol{\mu}(0)] \rangle \rho \\ & - \frac{A_0\omega_c}{4ec} \left(\frac{i}{\hbar} \right) \langle [\mathbf{Q}(t) \cdot \mathbf{k}, \boldsymbol{\varepsilon} \cdot \boldsymbol{\mu}(0)] \rangle \rho. \end{aligned} \quad (18')$$

Hereafter, we will consider two cases when the polarization properties of incident beam and detected signal field are specifically controlled to measure the optical activity of chiral molecule in solution.

III. RESPONSE FUNCTION OF OPTICAL ACTIVITY: CD AND ORD

The CD is characterized by the differential absorption, $\Delta A = A_{LCP} - A_{RCP}$, of LCP and RCP beams by chiral molecules, whereas the ORD the differential index of refraction, in other words, the circular birefringence, $\Delta n = n_L - n_R$. In the case of the frequency-domain CD spectroscopy, the absorbances A_{LCP} and A_{RCP} are separately measured and only

when the molecule under investigation is chiral, ΔA does not vanish. It is well known that the CD intensity is linearly proportional to the so-called rotational strength defined as $R_{eg} = \text{Im}[\boldsymbol{\mu}_{ge} \cdot \mathbf{M}_{eg}]$.¹ On the other hand, in the ORD spectroscopy, the optical rotation of linearly polarized beam caused by the circular birefringence is actually measured instead of Δn . In the present section, we will provide a time-domain description of the OA spectroscopy by considering the associated polarizations when the incident pulsed beam is controlled to be either LCP or RCP.

Without loss of generality, we will assume that the beam propagation direction is along the Z -axis in a space-fixed frame. Therefore, $\hat{\mathbf{k}} = \mathbf{k}/|\mathbf{k}| = \hat{\mathbf{z}}$. The X -component of the macroscopic polarization $P_x(t)$ can be directly detected by employing either spectral interferometric or upconversion detection method.³⁶ If the spectral interferometry is used to obtain the spectrum of $P_x(t)$, one can determine both the amplitude and phase of $P_x(t)$ as will be discussed later in this paper. On the other hand, if an upconversion technique is used, only the amplitude of $P_x(t)$ can be detected.

In order to derive expressions for $P_x(t)$ when the incident beam is either LCP or RCP, it is necessary to consider the radiation property of LCP and RCP beams first. The unit vectors of the LCP and RCP radiations are given as $\boldsymbol{\varepsilon}_L = (\hat{x} + i\hat{y})/\sqrt{2}$ and $\boldsymbol{\varepsilon}_R = (\hat{x} - i\hat{y})/\sqrt{2}$. Then, from the general expression for $\mathbf{P}(t)$ in Eq. (7) with Eq. (18), the $P_x(t)$'s for the LCP and RCP beams are found to be

$$P_x^{L,R}(t) = \frac{N}{V} \int_0^t d\tau \phi_x^{L,R}(t - \tau) F(\tau), \quad (19)$$

and

$$\begin{aligned} \phi_x^L(t) = & \frac{iA_0\omega_c}{2\sqrt{2}c} \left(\frac{i}{\hbar} \right) \langle [\mu_x(t), \mu_x(0) + i\mu_y(0)] \rangle \rho + \frac{iA_0\omega_c}{2\sqrt{2}c} \left(\frac{i}{\hbar} \right) \\ & \times \langle [\mu_x(t), M_y(0) - iM_x(0)] \rangle \rho + \frac{iA_0\omega_c}{2\sqrt{2}c} \left(\frac{i}{\hbar} \right) \\ & \times \langle [M_y(t), \mu_x(0) + i\mu_y(0)] \rangle \rho - \frac{A_0\omega_c^2}{4\sqrt{2}ec^2} \left(\frac{i}{\hbar} \right) \\ & \times \langle [\mu_x(t), Q_{xz}(0) + iQ_{yz}(0)] \rangle \rho - \frac{A_0\omega_c^2}{4\sqrt{2}ec^2} \left(\frac{i}{\hbar} \right) \\ & \times \langle [Q_{xz}(t), \mu_x(0) + i\mu_y(0)] \rangle \rho \\ \phi_x^R(t) = & \frac{iA_0\omega_c}{2\sqrt{2}c} \left(\frac{i}{\hbar} \right) \langle [\mu_x(t), \mu_x(0) - i\mu_y(0)] \rangle \rho + \frac{iA_0\omega_c}{2\sqrt{2}c} \left(\frac{i}{\hbar} \right) \\ & \times \langle [\mu_x(t), M_y(0) + iM_x(0)] \rangle \rho + \frac{iA_0\omega_c}{2\sqrt{2}c} \left(\frac{i}{\hbar} \right) \\ & \times \langle [M_y(t), \mu_x(0) - i\mu_y(0)] \rangle \rho - \frac{A_0\omega_c^2}{4\sqrt{2}ec^2} \left(\frac{i}{\hbar} \right) \\ & \times \langle [\mu_x(t), Q_{xz}(0) - iQ_{yz}(0)] \rangle \rho - \frac{A_0\omega_c^2}{4\sqrt{2}ec^2} \left(\frac{i}{\hbar} \right) \\ & \times \langle [Q_{xz}(t), \mu_x(0) - i\mu_y(0)] \rangle \rho. \end{aligned} \quad (20)$$

Therefore, the difference polarization $\Delta P_x(t)$, which is the

chiral polarization defined as $\Delta P_x(t) = P_x^L(t) - P_x^R(t)$, is found to be

$$\Delta P_x(t) = \frac{N}{V} \int_0^t d\tau \Delta \phi_x^{OA}(t - \tau) F(\tau), \quad (21)$$

with

$$\begin{aligned} \Delta \phi_x^{OA}(t) = & -\frac{A_0 \omega_c}{\sqrt{2}c} R_{xy}^{e-e}(t) + \frac{iA_0 \omega_c}{\sqrt{2}c} R_{xx}^{e-m}(t) \\ & - \frac{iA_0 \omega_c^2}{2\sqrt{2}ec^2} R_{xyz}^{e-q}(t), \end{aligned} \quad (22)$$

where

$$R_{xy}^{e-e}(t) = \left(\frac{i}{\hbar} \right) \langle [\mu_x(t), \mu_y(0)] \rho \rangle, \quad (23)$$

$$\begin{aligned} R_{xx}^{e-m}(t) = & \left(\frac{i}{\hbar} \right) \langle [\mu_x(t), -iM_x(0)] \rho \rangle \\ & + \left(\frac{i}{\hbar} \right) \langle [M_x(t), i\mu_x(0)] \rho \rangle, \end{aligned} \quad (24)$$

$$R_{xyz}^{e-q}(t) = \left(\frac{i}{\hbar} \right) \langle [\mu_x(t), Q_{yz}(0)] \rho \rangle + \left(\frac{i}{\hbar} \right) \langle [Q_{xz}(t), \mu_y(0)] \rho \rangle. \quad (25)$$

Here, $R_{ij}^{e-e}(t)$, $R_{ij}^{e-m}(t)$, and $R_{ijk}^{e-q}(t)$ indicate the electric dipole–electric dipole, the electric dipole–magnetic dipole, and the electric dipole–electric quadrupole response functions, respectively, and i , j , and k are the specific polarization directions.

The next step is to perform the rotational averaging of $\Delta P_x(t)$ for randomly oriented chiral molecules in an isotropic medium. Since the only rotationally invariant second- and third-rank tensors are the Kronecker delta and Levi–Civita epsilon, respectively,³⁷ the first term in Eq. (22) vanishes. Second, the third term also vanishes because the quadrupole tensor is symmetric whereas the Levi–Civita epsilon tensor is antisymmetric. Consequently, the time-domain chiral polarization associated with the optical activity is given as

$$\overline{\Delta P_x(t)} = \frac{N}{V} \left(\frac{iA_0 \omega_c}{\sqrt{2}c} \right) \int_0^t d\tau R_{xx}^{e-m}(t - \tau) F(\tau). \quad (26)$$

Note that the difference (chiral) polarization is determined by the electric dipole–magnetic dipole response function. One can make a connection of this result to the conventional differential expression for the OA.

IV. DIFFERENTIAL ABSORPTION COEFFICIENT AND CIRCULAR BIREFRINGENCE

The real and imaginary parts of the susceptibility are related to the frequency-dependent index of refraction and absorption coefficient, respectively. The absorbance associated with a transition from $|g\rangle$ to $|e\rangle$ state is linearly proportional to the dipole strength $\mu_{ge} \cdot \mu_{eg}$, whereas the OA intensity is to the rotational strength defined as $\text{Im}[\mu_{ge} \cdot \mathbf{M}_{eg}]$.

Now, from the polarizations in Eq. (19), one can obtain an expression for the frequency-dependent index of refraction and absorption coefficient by following the standard procedure. First of all, it should be noted that the amplitude of the vector potential is related to that of the electric field as $E_0 = i\omega_c A_0/c$. Also, by considering the rotational average of Eq. (20), the polarization $\overline{P_x^L}(t)$, which corresponds to the case when the incident beam is LCP and when the X-component of the polarization vector is detected, is given as

$$\overline{P_x^L}(t) = \frac{1}{\sqrt{2}} \int_0^t d\tau \chi_L(t - \tau) E(\tau), \quad (27)$$

where $E(t) = E_0 F(t)$ and

$$\chi_L(t) = \frac{N}{2V} \{R_{xx}^{e-e}(t) + R_{xx}^{e-m}(t)\}. \quad (28)$$

Defining the Fourier transform of $\chi_L(t)$ as

$$\chi_L(\omega) = \int_0^\infty d\tau \chi_L(t) e^{i\omega t} \quad (29)$$

and separating the real and imaginary parts of $\chi_L(\omega)$ as

$$\chi_L(\omega) = \chi_L'(\omega) + i\chi_L''(\omega), \quad (30)$$

we find

$$\chi_L'(\omega) = \frac{N}{2V} \int_0^\infty dt \{R_{xx}^{e-e}(t) + R_{xx}^{e-m}(t)\} \cos \omega t \quad (31)$$

$$\chi_L''(\omega) = \frac{N}{2V} \int_0^\infty dt \{R_{xx}^{e-e}(t) + R_{xx}^{e-m}(t)\} \sin \omega t. \quad (32)$$

By using the damped oscillator model, the response functions in Eq. (28) can be approximately written as

$$R_{xx}^{e-e}(t) = \sum_j \mu_{x,j}^2 e^{-\gamma_j t/2} \sin \omega_j t, \quad (33)$$

$$R_{xx}^{e-m}(t) = \sum_j \text{Im}[\mu_{x,j} M_{x,j}] e^{-\gamma_j t/2} \sin \omega_j t. \quad (34)$$

Here, the transition electric and magnetic dipole matrix elements are denoted as $\mu_{x,j}$ and $M_{x,j}$, respectively. The transition frequency and dephasing constant are ω_j and γ_j . Inserting Eqs. (33) and (34) into Eqs. (31) and (32), we have

$$\begin{aligned} \chi_L'(\omega) = & \frac{N}{4V} \sum_j \{ \mu_{x,j}^2 + \text{Im}[\mu_{x,j} M_{x,j}] \} \left(\frac{-(\omega - \omega_j)}{(\omega - \omega_j)^2 + \gamma_j^2/4} \right. \\ & \left. + \frac{(\omega + \omega_j)}{(\omega + \omega_j)^2 + \gamma_j^2/4} \right), \end{aligned} \quad (35)$$

$$\begin{aligned} \chi_L''(\omega) = & \frac{N}{4V} \sum_j \{ \mu_{x,j}^2 + \text{Im}[\mu_{x,j} M_{x,j}] \} \left(\frac{\gamma_j/2}{(\omega - \omega_j)^2 + \gamma_j^2/4} \right. \\ & \left. - \frac{\gamma_j/2}{(\omega + \omega_j)^2 + \gamma_j^2/4} \right). \end{aligned} \quad (36)$$

Usually, $\mu_{x,j}^2 \gg \text{Im}[\mu_{x,j} M_{x,j}]$ so that the absorption coefficient is determined by the dipole strength. One can obtain the

similar expression for $\chi'_R(\omega)$ and $\chi''_R(\omega)$, which are identical to Eqs. (35) and (36), respectively, and except that the sign of $\text{Im}[\mu_{x,j}M_{x,j}]$ changes. For $1+4\pi\chi'_{L,R}(\omega) \gg 4\pi\chi''_{L,R}(\omega)$, the indices of refraction of LCP and RCP are given by $n_{L,R}(\omega) = [1+4\pi\chi'_{L,R}(\omega)]^{1/2}$ and thus the circular birefringence, $\Delta n(\omega) = n_L - n_R$, can be expressed as

$$\begin{aligned} \Delta n(\omega) &= \frac{2\pi}{n(\omega)} \{\chi'_L(\omega) - \chi'_R(\omega)\} \\ &= \frac{\pi N}{n(\omega)V} \sum_j \left\{ \text{Im}[\mu_{x,j}M_{x,j}] \left(\frac{-(\omega - \omega_j)}{(\omega - \omega_j)^2 + \gamma_j^2/4} \right. \right. \\ &\quad \left. \left. + \frac{(\omega + \omega_j)}{(\omega + \omega_j)^2 + \gamma_j^2/4} \right) \right\}, \end{aligned} \quad (37)$$

where $n(\omega)$ is the mean index of refraction. Within the rotating wave approximation, only the first term is taken to describe the circular birefringence in the positive frequency range as

$$\Delta n(\omega) = \frac{-\pi N}{n(\omega)V} \sum_j \text{Im}[\mu_{x,j}M_{x,j}] \frac{\omega - \omega_j}{(\omega - \omega_j)^2 + \gamma_j^2/4}. \quad (38)$$

Next, let us consider the differential absorption coefficient. From the definition of the absorption coefficient,³⁵

$$\kappa_a(\omega) = \frac{4\pi\omega}{n(\omega)c} \chi''(\omega), \quad (39)$$

and similarly, we confirm that the CD spectrum, which is the difference between the two absorption coefficients of chiral molecules for LCP and RCP beams, is given as

$$\begin{aligned} \Delta\kappa_a(\omega) &= \frac{4\pi\omega}{n(\omega)c} \{\chi''_L(\omega) - \chi''_R(\omega)\} \\ &= \frac{\sqrt{2}\pi\omega N}{n(\omega)cV} \sum_j \text{Im}[\mu_{x,j}M_{x,j}] \frac{\gamma_j/2}{(\omega - \omega_j)^2 + \gamma_j^2/4}. \end{aligned} \quad (40)$$

If the transition electric and magnetic dipole vectors in a molecule-fixed frame are denoted as $\boldsymbol{\mu}_j^M$ and \mathbf{M}_j^M , respectively, one can rewrite $\text{Im}[\mu_{x,j}M_{x,j}]$ as $(1/3)\text{Im}[\boldsymbol{\mu}_j^M \cdot \mathbf{M}_j^M]$ so that

$$\Delta\kappa_a(\omega) = \frac{\sqrt{2}\pi\omega N}{3n(\omega)cV} \sum_j \text{Im}[\boldsymbol{\mu}_j^M \cdot \mathbf{M}_j^M] \frac{\gamma_j/2}{(\omega - \omega_j)^2 + \gamma_j^2/4}. \quad (41)$$

One can use different models for dephasing process such as inhomogeneous line broadening, Kubo theory, Brownian oscillator model,³⁵ bilinearly coupled harmonic oscillator bath model,³⁸ etc., but the main features revealed by Eq. (41) remain the same. The results in this section will be directly compared to the novel cross-polarization measurement method for time-resolved OA spectroscopy discussed in the following section.

V. PERPENDICULAR DETECTION METHOD FOR OA MEASUREMENT

In practice, when a CD experiment is performed one should measure the difference in absorbance of LCP and

RCP beams. Typically, the CD signal intensity is four to six orders of magnitude smaller than the electric-dipole-allowed absorbance. Consequently, it was necessary to accumulate a large number of data to obtain a statistically meaningful CD spectrum. Using the conventional spectrometer, one cannot perform an ultrafast time-resolved CD experiment. Kliger and co-workers therefore used an ellipsometric detection scheme to carry out time-resolved CD measurement. However, the time resolution reached by this technique is in nano-second timescale. Therefore, any dynamical event involving changes of molecular chirality with timescale faster than that could not be studied by using the method. In the case of VCD or vibrational ORD (VORD), the detection of vibrational OA (VOA) signal is even more challenging due to the low sensitivity of IR detector, which prohibits a systematic development of time-resolved VOA spectroscopy.

In this section, we will show that by measuring the perpendicular FID polarization component with respect to the incident beam polarization direction,^{31,32,39,40} one can obtain both the CD and ORD spectra simultaneously by taking the Fourier transform of the measured polarization, by dispersing the polarization directly with monochromator, or by using the multichannel array detector coupled with a dispersive device. A detailed experimental scheme proposed will be discussed later. The incident beam propagation direction is again assumed to be along the Z-axis in a space-fixed frame, i.e., $\hat{\mathbf{k}} = \mathbf{k}/|\mathbf{k}| = \hat{\mathbf{z}}$. Unlike the case of the conventional CD spectroscopy utilizing both LCP and RCP beams, the incident beam for the present case is linearly polarized and its polarization direction is parallel to the Y-axis, $\boldsymbol{\varepsilon} = \hat{\mathbf{y}}$. After the optical sample cell, another linear polarizer is placed to select the X-component of the macroscopic polarization vector $P_x(t)$. Therefore, the incident beam polarization is perpendicular to the detected macroscopic polarization $P_x(t)$ so that this experimental scheme will be denoted as a cross-polarization detection (CPD) method. With this beam configuration, we find that $P_x^{CPD}(t)$ is given as

$$P_x^{CPD}(t) = \frac{N}{V} \int_0^t d\tau \phi_x^{CPD}(t - \tau) F(\tau), \quad (42)$$

where

$$\phi_x^{CPD}(t) = \frac{iA_0\omega_c}{2c} R_{xy}^{e-e}(t) + \frac{A_0\omega_c}{2c} R_{xx}^{e-m}(t) - \frac{A_0\omega_c^2}{4ec^2} R_{xyz}^{e-q}(t). \quad (43)$$

The rotational averaged polarization $\bar{P}_x^{CPD}(t)$ is then found to be determined by the electric dipole-magnetic dipole term as

$$\bar{P}_x^{CPD}(t) = \frac{N}{V} \left(\frac{A_0\omega_c}{2c} \right) \int_0^t d\tau R_{xx}^{e-m}(t - \tau) F(\tau). \quad (44)$$

Note that the CPD polarization is linearly proportional to the chiral polarization given in Eq. (26) as

$$\sqrt{2}i\bar{P}_x^{CPD}(t) = \Delta\bar{P}_x(t). \quad (45)$$

This is an important result showing that the CPD method can be used to measure the CD polarization directly and that the two differ from each other by the constant of $\sqrt{2}$ and the

phase factor $\exp(i\pi/2)(=i)$. As mentioned above, the CPD method does not require a subtraction of two separately measured polarizations (or absorbances) with LCP and RCP beams. Therefore, one can achieve an ultrafast (femtosecond) measurement of CD spectrum when an appropriate heterodyne-detection method is used.

In addition to the CPD polarization mentioned above, we will focus on another rotationally averaged polarization component $\overline{P}_y(t)$, which is related to the electric dipole–electric dipole response function, that is, the conventional optical FID. The polarization direction of the incident beam is the same as the case of the CPD scheme, but the second linear polarizer after the sample cell is deliberately aligned to transmit the Y -component of the polarization generated from the sample. With this geometry, we find that $P_y(t)$ is given as

$$P_y(t) = \frac{N}{V} \int_0^t d\tau \phi_y(t-\tau) F(\tau), \quad (46)$$

where

$$\phi_y(t) = \frac{iA_0\omega_c}{2c} R_{yy}^{e-e}(t) + \frac{A_0\omega_c}{2c} R_{yx}^{e-m}(t) - \frac{A_0\omega_c^2}{4ec^2} R_{yyz}^{e-q}(t). \quad (47)$$

The rotational averaged polarization $\overline{P}_y(t)$ is then found to be as

$$\overline{P}_y(t) = \frac{N}{V} \left(\frac{iA_0\omega_c}{2c} \right) \int_0^t d\tau R_{yy}^{e-e}(t-\tau) F(\tau). \quad (48)$$

This result will be used to show how to retrieve the weak OA FID polarization from the spectral interferometric measurement.

VI. EMITTED SIGNAL ELECTRIC FIELD AND SPECTRAL INTERFEROMETRY

The generated FID polarizations, $\overline{P}_y(t)$ and $\overline{P}_x(t)$, of which Fourier transforms are related to the absorption (and dispersion) and CD (and ORD) spectra, respectively, are the sources of generated electric fields that obey the Maxwell equation. For the transverse component of the emitted signal electric field $\mathbf{E}_s(z,t)$ propagating along the z -direction, the coupled Maxwell equation is given as

$$\nabla^2 \mathbf{E}_s(z,t) - \frac{1}{c^2} \frac{\partial^2}{\partial t^2} \mathbf{E}_s(z,t) = \frac{4\pi}{c^2} \frac{\partial^2}{\partial t^2} \overline{\mathbf{P}}_s(z,t). \quad (49)$$

Here, $\mathbf{E}_s(z,t)$ and the rotationally averaged polarization, $\overline{\mathbf{P}}_s(z,t)$, can be expressed as their respective X - Y -components, which are given by

$$\mathbf{E}_s(z,t) = E_s^x(z,t)\hat{x} + E_s^y(z,t)\hat{y}, \quad (50)$$

$$\overline{\mathbf{P}}_s(z,t) = \overline{P}_x(z,t)\hat{x} + \overline{P}_y(z,t)\hat{y}, \quad (51)$$

where

$$\begin{aligned} \overline{P}_x(z,t) &= \left(\frac{-iN}{2V} \right) \int_0^t d\tau R_{xx}^{e-m}(t-\tau) E_s^y(z,\tau) \\ &+ \left(\frac{N}{2V} \right) \int_0^t d\tau R_{xx}^{e-e}(t-\tau) E_s^x(z,\tau), \end{aligned} \quad (52)$$

$$\begin{aligned} \overline{P}_y(z,t) &= \left(\frac{N}{2V} \right) \int_0^t d\tau R_{yy}^{e-e}(t-\tau) E_s^y(z,\tau) \\ &+ \left(\frac{iN}{2V} \right) \int_0^t d\tau R_{yy}^{e-m}(t-\tau) E_s^x(z,\tau). \end{aligned} \quad (53)$$

The second term in Eq. (53) represents the electric dipole–magnetic dipole response induced by the X -component of the generated electric field at z position, and it can be ignored not only because $E_s^x(z,t)$, which is related to the OA FID field, is much smaller than $E_s^y(z,t)$, but also because the electric dipole–magnetic dipole response function $R_{yy}^{e-m}(t)$ is much smaller than the electric dipole–electric dipole response function $R_{yy}^{e-e}(t)$. On the other hand, the second term in Eq. (52) cannot be neglected because the relative magnitude of $R_{xx}^{e-e}(t)$ with respect to $R_{xx}^{e-m}(t)$ is quite large even though $E_s^x(z,t)$ is much smaller than $E_s^y(z,t)$. Taking into consideration of these facts, one can rewrite the coupled Maxwell equation separately as

$$\begin{aligned} \nabla^2 E_s^x(z,t) - \frac{1}{c^2} \frac{\partial^2}{\partial t^2} E_s^x(z,t) \\ = \frac{4\pi}{c^2} \frac{\partial^2}{\partial t^2} \left[\left(\frac{-iN}{2V} \right) \int_0^t d\tau R_{xx}^{e-m}(t-\tau) E_s^y(z,\tau) \right. \\ \left. + \left(\frac{N}{2V} \right) \int_0^t d\tau R_{xx}^{e-e}(t-\tau) E_s^x(z,\tau) \right], \end{aligned} \quad (54)$$

$$\begin{aligned} \nabla^2 E_s^y(z,t) - \frac{1}{c^2} \frac{\partial^2}{\partial t^2} E_s^y(z,t) \\ \cong \frac{4\pi}{c^2} \frac{\partial^2}{\partial t^2} \left(\frac{N}{2V} \right) \int_0^t d\tau R_{yy}^{e-e}(t-\tau) E_s^y(z,\tau). \end{aligned} \quad (55)$$

By Fourier transforming Eq. (55), one can easily solve it in the frequency domain and, we find that

$$E_s^y(z,\omega) \cong E_s^y(0,\omega) \exp(ik'z), \quad (56)$$

where

$$E_s^y(0,\omega) = \int_0^\infty dt E_0 f(t) e^{i(\omega-\omega_0)t}, \quad (57)$$

$$k'(\omega) = \frac{\omega}{c} [1 + 4\pi\chi(\omega)]^{1/2}. \quad (58)$$

Here, $\chi(\omega)$ is the linear susceptibility, i.e.,

$$\chi(\omega) = \int_0^\infty dt \chi(t) e^{i\omega t}, \quad (59)$$

where

$$\chi(t) = \frac{N}{2V} R_{yy}^{e-e}(t). \quad (60)$$

Now, one can obtain the X -component of the emitted signal electric field $E_s^x(z,t)$ at z position, which corresponds to the OA FID field, by solving Eq. (54) with $E_s^y(z,\omega)$ in Eq. (56). By invoking the slowly varying-amplitude approximation

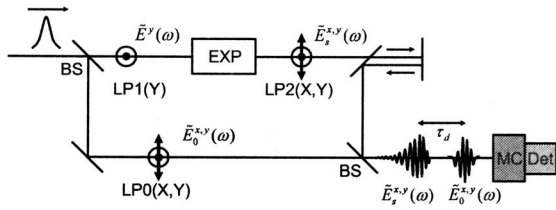


FIG. 1. Experimental setup for FTSI, based on a Mach-Zehnder interferometer. The incident laser pulse is linearly polarized along the Y-axis before it enters into the sample cell. The second linear polarizer is placed after the cell to select the X- or Y-polarized signal field. The reference pulse is X- or Y-polarized and it precedes the signal field by a finite time t_d ; BS, beam splitter; LP0-2, linear polarizers; MC, monochromator; Det, multichannel array detector.

and Fourier transforming both sides of Eq. (54), the equation can be rewritten as

$$ik' \frac{\partial}{\partial z} E_0^x(z, \omega) \cong \frac{\pi i \omega^2}{c^2} \Delta\chi(\omega) E_0^y(\omega), \quad (61)$$

where

$$\Delta\chi(\omega) \equiv \chi_L(\omega) - \chi_R(\omega) = \int_0^\infty dt \left(\frac{N}{V} \right) R_{xx}^{e-m}(t) e^{i\omega t}, \quad (62)$$

and $E_0^x(z, \omega)$ and $E_0^y(\omega)$ are the amplitudes of the X- and Y-components of the electric field, respectively. For $1 + 4\pi\chi'(\omega) \gg 4\pi\chi''(\omega)$, the emitted OA FID field after passing through the sample with length L is given as

$$\tilde{E}_s^x(L, \omega) \cong \frac{\pi\omega L}{cn(\omega)} \Delta\chi(\omega) \tilde{E}_s^y(L, \omega). \quad (63)$$

This is the principal result of this paper. It shows that the complex susceptibility containing information on the CD and ORD can be obtained by measuring the two electric field spectra $\tilde{E}_s^x(\omega)$ and $\tilde{E}_s^y(\omega)$.

From the relationship in Eq. (63), the CD (ΔA) and ORD ($\Delta\varphi$) spectra can be retrieved from the measurements of the X- and Y-components of the generated signal field $\mathbf{E}_s(\omega)$ as

$$\begin{aligned} \Delta A(\omega) &= \frac{\Delta\kappa_a(\omega)L}{2.303} = \frac{4\pi\omega L}{2.303n(\omega)c} \text{Im}[\Delta\chi(\omega)] \\ &= \frac{4}{2.303} \text{Im} \left[\frac{\tilde{E}_s^x(\omega)}{\tilde{E}_s^y(\omega)} \right], \end{aligned} \quad (64)$$

$$\begin{aligned} \Delta\varphi(\omega) &= \frac{\Delta n(\omega)\omega L}{2c} = \frac{\pi\omega L}{n(\omega)c} \text{Re}[\Delta\chi(\omega)] \\ &= \frac{\sqrt{2}}{2} \text{Re} \left[\frac{\tilde{E}_s^x(\omega)}{\tilde{E}_s^y(\omega)} \right]. \end{aligned} \quad (65)$$

Note that the optical rotation angle is defined as a half of the phase change between LCP and RCP after passing through the sample length L .

Now, let us consider the Fourier transform spectral interferometric (FTSI) detection of the emitted electric fields in Eqs. (56) and (63) by using the Mach-Zehnder interferometer (Fig. 1). Although a related wave-packet interferometric method has been shown to be useful in obtaining amplitude-

level information on nuclear wave packets for electronic chromophores,⁴¹⁻⁴⁴ the FTSI method has been shown to be quite versatile and easy to implement in a variety of linear and nonlinear optical signal field detections. The incident pulse is separated into two parts. For the measurement of $\tilde{E}_s^y(\omega)$, the Y-polarized pulse is injected into the solution sample containing chiral molecules and the Y-polarized emitted FID signal field is selected by using two linear polarizers (LP1, LP2) that are placed before and after the sample cell. A translational stage is used to deliberately delay the FID signal field with respect to the reference field $\tilde{E}_0(\omega)$. In the second arm of the Mach-Zehnder interferometer, another linear polarizer (LP0) is placed to make the reference pulse being polarized along the Y-direction.

Second, for the measurement of $\tilde{E}_s^x(\omega)$, the LP2 and the LP0 are rotated to the X-axis with the LP1 being Y-polarized and only the X-polarized FID field is detected. The reference pulse and X- or Y-polarized FID signal field are added together and the total signals are dispersed to measure the entire spectra. In the present FTSI heterodyne-detection measurement, $\tilde{E}_s^{x,y}(\omega)$ and $\tilde{E}_0(\omega)$ are the FID signal fields and the reference pulse spectra, respectively. The signal detected at the output of the spectrometer reads

$$\begin{aligned} S^{x,y}(\omega) &= |\tilde{E}_0(\omega) + \tilde{E}_s^{x,y}(\omega)|^2 = |\tilde{E}_0(\omega)|^2 + |\tilde{E}_s^{x,y}(\omega)|^2 \\ &\quad + 2 \text{Re}[\tilde{E}_0^*(\omega) \tilde{E}_s^{x,y}(\omega)]. \end{aligned} \quad (66)$$

The advantages of frequency-domain interferometry over time-domain interferometry are (1) that the entire interferogram can be recorded simultaneously by using an multichannel array detector and (2) that small fluctuations of the optical path do not validate the interferogram. The use of shutters on both arms of the interferometer allows us to subtract out background signals and to record the interference part only, i.e.,

$$S_h^{x,y}(\omega) = 2 \text{Re}[\tilde{E}_0^*(\omega) \tilde{E}_s^{x,y}(\omega)]. \quad (67)$$

As experimentally and theoretically shown by Joffe and co-workers, one can use a time-separated reference pulse to obtain the amplitude and phase information on $E_s^{x,y}(t)$, which is complex.¹⁸ The reference pulse precedes the signal by a fixed time delay τ_d . The time delay should be sufficiently large that the overlap between the reference pulse and signal field can be ignored, but it should be small enough to make the interference signal measurable. In that case, the interference part of the measured signal is

$$S_h^{x,y}(\omega) = 2 \text{Re}[\tilde{E}_0^*(\omega) \tilde{E}_s^{x,y}(\omega) \exp(i\omega\tau_d)]. \quad (68)$$

Then, the signal field $E_s^{x,y}(\omega)$ can be obtained as

$$\tilde{E}_s^{x,y}(\omega) = \frac{F[\theta(t)F^{-1}\{S_h^{x,y}(\omega)\}]\exp(-i\omega\tau_d)}{2\tilde{E}_0^*(\omega)}, \quad (69)$$

where $F(\dots)$ and $F^{-1}(\dots)$ represent the Fourier and inverse Fourier transformations, respectively, and $\theta(t)$ is the Heavyside step function. The reason why the Heavyside step function is multiplied to the time-domain heterodyne-detected signal $F^{-1}\{S_h^{x,y}(\omega)\}$ is to obtain the complex function

$\tilde{E}_0^*(\omega)\tilde{E}_s^{x,y}(\omega)\exp(i\omega\tau_d)$ in Eq. (68), by Fourier transforming $\theta(t)F^{-1}\{S_h^{x,y}(\omega)\}$. Note that the terms on the right-hand side of Eq. (69) are experimentally measured functions. Then, combining Eqs. (64) and (65) with Eq. (69), we have

$$\Delta A(\omega) = \frac{4}{2.303} \text{Im} \left[\frac{F[\theta(t)F^{-1}\{S_h^x(\omega)\}]}{F[\theta(t)F^{-1}\{S_h^y(\omega)\}]} \right], \quad (70)$$

$$\Delta\varphi(\omega) = \frac{\sqrt{2}}{2} \text{Re} \left[\frac{F[\theta(t)F^{-1}\{S_h^x(\omega)\}]}{F[\theta(t)F^{-1}\{S_h^y(\omega)\}]} \right]. \quad (71)$$

This result shows how one can combine the CPD method with the FTSI to measure the snapshot CD and ORD spectra in femtosecond timescale.

VII. NUMERICAL SIMULATION STUDY

In order to demonstrate the experimental possibility, we present a numerical simulation study for a model system. It is assumed that the IR absorption spectrum in the frequency range of interest consists of three normal mode transitions as can be seen in Fig. 2(a). The IR and VOA response functions are

$$R_{yy}^{e-e}(t) = \sum_{j=1}^3 \mu_{y,j}^2 e^{-\gamma_j t/2} \sin \omega_j t, \quad (72)$$

$$R_{xx}^{e-m} = \sum_{j=1}^3 \text{Im}[\mu_{x,j} M_{x,j}] e^{-\gamma_j t/2} \sin \omega_j t. \quad (73)$$

The three normal mode frequencies are 2900, 2950, and 3000 cm^{-1} and the associated dephasing constants (γ_j) are 0.006, 0.004, and 0.004 fs^{-1} . The ratios of the dipole strengths for the three modes are 1:0.5:0.3. Since we assumed exponential dephasing processes for the IR free induction decay [see Eq. (72)], the lineshape of each individual peak is given as a Lorentzian function. One can use different dephasing models, but the main results do not depend on the detailed dephasing model. The concentration (N/V) and path length (L) of the sample and the absolute dipole strengths used in the simulations were appropriately set such that the absorbance at 2900 cm^{-1} is about 1. The corresponding VCD spectrum (ΔA) is shown in Fig. 2(b). It is assumed that the rotational strengths of the three peaks have different amplitudes and signs and they are -1×10^{-5} , 0.5×10^{-5} , and -0.3×10^{-5} relative to the dipole strengths, respectively. Note that for the vibrational transition, the rotational strength is typically four to six orders of magnitude smaller than the dipole strength.

In order to carry out the spectral interferometric detections of IR FID as well as VOA FID, one should use a reference pulse of which temporal intensity envelop is assumed to be Gaussian with full width at half maximum of 100 fs (with respect to intensity profile) and center frequency of 2950 cm^{-1} . Its Fourier-transformed spectrum $E_0(\omega)$ is also Gaussian and shown in Fig. 2(c). An incident pulse $E^y(0,t)$ before the sample, which creates vibrational coherence in the sample, is also assumed to have the same tempo-

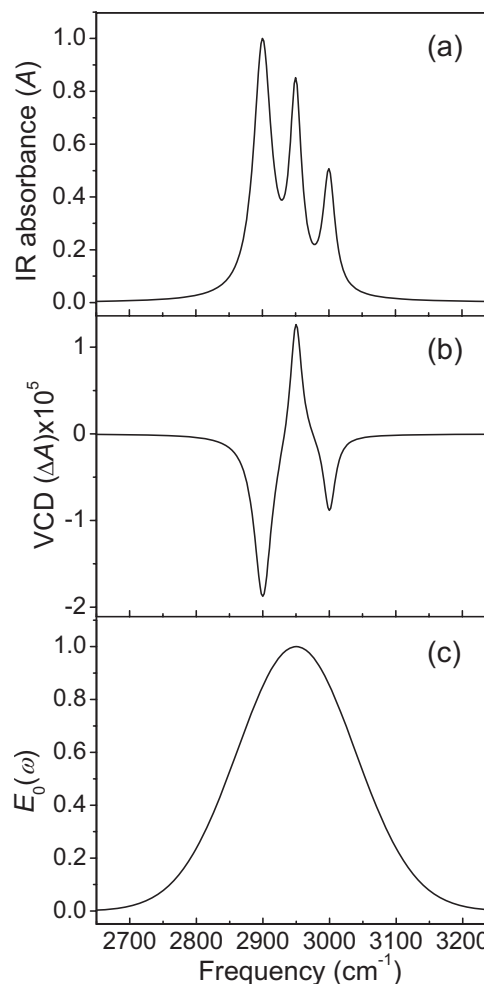


FIG. 2. (a) Absorption spectrum of the model system. The three normal mode frequencies are assumed to be 2900, 2950, and 3000 cm^{-1} . The corresponding dephasing constants (γ_j) are 0.006, 0.004, and 0.004 fs^{-1} , respectively. The relative dipole strengths determining the IR peak intensity are 1, 0.5, and 0.3, respectively. (b) The VCD spectrum. The relative rotational strengths are assumed to be -1×10^{-5} , 0.5×10^{-5} , and -0.3×10^{-5} , respectively. (c) The Fourier-transformed spectrum of the reference pulse $\tilde{E}_0(\omega)$.

ral and spectral profiles as the reference pulse, and any distortion of its temporal shape by other optics does not occur.

As shown in Eq. (70), to obtain the CD spectrum $\Delta A(\omega)$, one should first perform a heterodyned detection in a parallel polarizer configuration where both LP1 and LP2 are Y -polarized, from which $F[\theta(t)F^{-1}\{S_h^y(\omega)\}]$ associated with the IR FID field can be obtained. Strictly speaking, the $E_s^y(\omega)$ field is not the IR FID field, but the interference field between the IR FID and the incident pulse. Since the IR FID field destructively interferes with the incident pulse due to the absorption process, the $E_s^y(\omega)$ field is actually the *transmitted* field of the incident pulse through the sample. For the sake of notational simplicity, we will just denote it as the IR FID field hereafter.

When the delay time τ_d between the reference pulse and signal field for the FTSI measurement is set to 1 ps, the spectral interferogram of the IR FID and the reference pulse, $S_h^y(\omega) = 2 \text{Re}[\tilde{E}_0^*(\omega)\tilde{E}_s^y(\omega)\exp(i\omega\tau_d)]$, was calculated and is plotted in Fig. 3(a) (the solid line). For the VOA FID

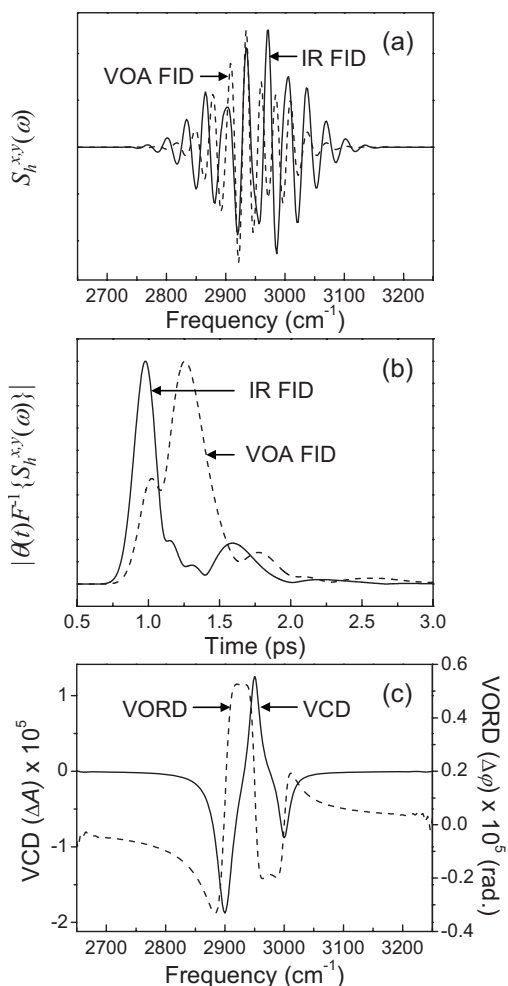


FIG. 3. (a) Normalized heterodyne-detected spectral interferograms of IR $S_h^y(\omega)$, (solid line) and VOA FID $S_h^x(\omega)$, and (dashed line) signal fields. Note that the relative magnitudes of the spectral interferograms for IR and VOA FID signals are about 1 and 5×10^{-6} , respectively, before normalizing them. (b) Normalized time-domain interference signal amplitudes obtained by calculating $|\theta(t)F^{-1}\{S_h^{x,y}(\omega)\}|$. (c) The VCD (solid line, left scale) and VORD (dashed line, right scale) spectra retrieved from the spectral interferograms of IR and VOA FID signal fields.

only in Eq. (63), one can similarly calculate $S_h^x(\omega) = 2 \operatorname{Re}[\tilde{E}_0^*(\omega)\tilde{E}_s^x(\omega)\exp(i\omega\tau_d)]$ [the dashed line in Fig. 3(a)]. The two spectral interferograms shown in Fig. 3(a) are normalized and the relative magnitudes of the $S_h^y(\omega)$ and $S_h^x(\omega)$ are about 1 and 5×10^{-6} , respectively, before normalizing them. It is noted that not only the amplitudes but also the relative phases of interferometric peaks in the $S_h^y(\omega)$ and $S_h^x(\omega)$ are different from one another. The $|\theta(t)F^{-1}\{S_h^{x,y}(\omega)\}|$'s for the IR (the solid line) and VOA FID (the dashed line) in Fig. 3(b) also have different temporal shapes with respect to each other.

As shown in the previous section [Eqs. (70) and (71)], one can retrieve not only the VCD (ΔA) but also the VORD ($\Delta\varphi$) spectra by analyzing these spectral interferograms obtained from both X - and Y -polarized detection geometries, and such extracted spectra are plotted in Fig. 3(c). It is noteworthy that the retrieved VCD spectrum (solid line) in Fig. 3(c) is exactly the same as that shown in Fig. 2(b), and the resonant VORD spectrum (dashed line) is also quantitatively obtained without additional measurement of

frequency-dependent optical rotation angle or Kramers–Kronig transformation. An additional advantage of the present X - and Y -polarized detection method is that one does not have to accurately determine the amplitude and phase of the reference pulse nor to precisely estimate the time delay between the signal field and the reference pulse as long as the two interferometer arms are sufficiently stable (in terms of phase fluctuation) so that the time delay τ_d is unchanged during the measurements.

VIII. SUMMARY

In this paper, a theoretical description of femtosecond CD spectroscopy utilizing spectral interferometric heterodyne-detection technique was presented. Considering the magnetic dipole–magnetic field and electric quadrupole–electric field interactions in addition to the electric dipole–electric field interaction, we developed a linear response theory for the CD (and also ORD) and found that the cross-polarization geometry can be used to selectively measure the phase and amplitude of the optical activity free induction decay field. Inserting the crossed linear polarizers before and after the sample cell and allowing the OA FID field interfering with reference pulse, one can measure the OA FID spectral interferogram with a properly chosen multichannel array detector. An absolute retrieval of the CD and ORD spectra can be achieved by the measurements of both X - and Y -polarized signal fields because the detected X -polarized signal field obtained by solving the coupled Maxwell equation is related to the generated Y -polarized field (the IR FID). For a model system with three normal modes, we carried out numerical simulations of various observables for the Fourier-transform OA FID spectroscopy operating in femtosecond time scale. We finally showed that the VOA FID signal field along with the IR FID field can be measured via the heterodyned spectral interferometric method to simultaneously extract the CD and ORD spectra from their spectral interferograms.

ACKNOWLEDGMENTS

This work was supported by Creative Research Initiatives (CMDI) of MEST/KOSEF. H.R. thanks Dr. Jonggu Jeon for stimulating discussions.

- N. Berova, K. Nakanishi, and R. W. Woody, *Circular Dichroism: Principles and Applications* (Wiley, New York, 2000).
- C. F. Zhang, J. W. Lewis, R. Cerpa, I. D. Kuntz, and D. S. Kliger, *J. Phys. Chem.* **97**, 5499 (1993).
- E. Chen, M. J. Wood, A. L. Fink, and D. S. Kliger, *Biochemistry* **37**, 5589 (1998).
- D. J. Vitale, R. A. Goldbeck, D. B. Kim-Shapiro, R. M. Esquerra, L. J. Parkhurst, and D. S. Kliger, *Biochemistry* **39**, 7145 (2000).
- T. Dartigalongue and F. Hache, *Chem. Phys. Lett.* **415**, 313 (2005).
- X. Xie and J. D. Simon, *J. Am. Chem. Soc.* **112**, 7802 (1990).
- G. A. Ellove, A. F. Chaffotte, H. Roder, and M. E. Goldberg, *Biochemistry* **31**, 6876 (1992).
- J. W. Lewis, R. A. Goldbeck, D. S. Kliger, X. Xie, R. C. Dunn, and J. D. Simon, *J. Phys. Chem.* **96**, 5243 (1992).
- E. Chen, W. Parker, J. W. Lewis, P. S. Song, and D. S. Kliger, *J. Am. Chem. Soc.* **115**, 9854 (1993).
- D. B. Shapiro, R. A. Goldbeck, D. Che, R. M. Esquerra, S. J. Paquette, and D. S. Kliger, *Biophys. J.* **68**, 326 (1995).
- E. Chen, R. A. Goldbeck, and D. S. Kliger, *J. Am. Chem. Soc.* **126**,

- 11175 (2004).
- ¹²R. M. Esquerria, R. A. Goldbeck, D. B. Kim-Shapiro, and D. S. Kliger, *J. Phys. Chem. A* **102**, 8740 (1998).
- ¹³X. Xie and J. D. Simon, *Rev. Sci. Instrum.* **60**, 2614 (1989).
- ¹⁴C. Niezborala and F. Hache, *J. Opt. Soc. Am. B* **23**, 2418 (2006).
- ¹⁵F. Reynaud, F. Salin, and A. Barthelemy, *Opt. Lett.* **14**, 275 (1989).
- ¹⁶E. Tokunaga, A. Terasaki, and T. Kobayashi, *Opt. Lett.* **18**, 370 (1993).
- ¹⁷J.-P. Geindre, P. Audebert, A. Rousse, F. Fallières, J. C. Gauthier, A. Mysyrowicz, A. D. Santos, G. Hamoniaux, and A. Antonetti, *Opt. Lett.* **19**, 1997 (1994).
- ¹⁸L. Lepetit, G. Chériaux, and M. Joffre, *J. Opt. Soc. Am. B* **12**, 2467 (1995).
- ¹⁹D. N. Fittinghoff, J. L. Bowie, J. N. Sweetser, R. T. Jennings, M. A. Krumbugel, K. W. DeLong, R. Trebino, and I. A. Walmsley, *Opt. Lett.* **21**, 884 (1996).
- ²⁰J.-P. Likforman, M. Joffre, and V. Thierry-Mieg, *Opt. Lett.* **22**, 1104 (1997).
- ²¹W. J. Walecki, D. N. Fittinghoff, A. L. Smirl, and R. Trebino, *Opt. Lett.* **22**, 81 (1997).
- ²²S. M. Gallagher, A. W. Albrecht, J. D. Hybl, B. L. Landin, B. Rajaram, and D. M. Jonas, *J. Opt. Soc. Am. B* **15**, 2338 (1998).
- ²³C. Dorrer and F. Salin, *J. Opt. Soc. Am. B* **15**, 2331 (1998).
- ²⁴T. Brixner, I. V. Stiopkin, and G. R. Fleming, *Opt. Lett.* **29**, 884 (2004).
- ²⁵T. Brixner, J. Stenger, H. M. Vaswani, M. Cho, R. E. Blankenship, and G. R. Fleming, *Nature (London)* **434**, 625 (2005).
- ²⁶Y. S. Kim, J. Wang, and R. M. Hochstrasser, *J. Phys. Chem. B* **109**, 7511 (2005).
- ²⁷T. H. Zhang, C. N. Borca, X. Li, and S. T. Cundiff, *Opt. Express* **13**, 7432 (2005).
- ²⁸S.-H. Lim, A. G. Caster, and S. R. Leone, *Opt. Lett.* **32**, 1332 (2007).
- ²⁹M. T. Zanni, N.-H. Ge, Y. S. Kim, and R. M. Hochstrasser, *Proc. Natl. Acad. Sci. U.S.A.* **98**, 11265 (2001).
- ³⁰M. Khalil, N. Demirdoven, and A. Tokmakoff, *J. Phys. Chem. A* **107**, 5258 (2003).
- ³¹D. Abramavicius and S. Mukamel, *J. Chem. Phys.* **122**, 134305 (2005).
- ³²D. Abramavicius and S. Mukamel, *J. Chem. Phys.* **124**, 034113 (2006).
- ³³M. Cho, T. Brixner, I. Stiopkin, H. Vaswani, and G. R. Fleming, *J. Chin. Chem. Soc. (Taipei)* **53**, 15 (2006).
- ³⁴R. Loudon, *The Quantum Theory of Light* (Clarendon, Oxford, 1983).
- ³⁵S. Mukamel, *Principles of Nonlinear Optical Spectroscopy* (Oxford University Press, New York, 1995).
- ³⁶R. A. Crowell, G. R. Holtom, and X. S. Xie, *J. Phys. Chem.* **99**, 1840 (1995).
- ³⁷D. P. Craig and T. Thirunamachandran, *Molecular Quantum Electrodynamics: An Introduction to Radiation Molecule Interactions* (Dover, New York, 1998).
- ³⁸G. R. Fleming and M. Cho, *Annu. Rev. Phys. Chem.* **47**, 109 (1996).
- ³⁹J.-H. Choi and M. Cho, *J. Chem. Phys.* **127**, 024507 (2007).
- ⁴⁰M. Cho, *J. Chem. Phys.* **119**, 7003 (2003).
- ⁴¹S. Ramos-Sánchez and V. Romero-Rochín, *J. Chem. Phys.* **121**, 2117 (2004).
- ⁴²T. S. Humble and J. A. Cina, *Phys. Rev. Lett.* **93**, 060402 (2004).
- ⁴³T. S. Humble and J. A. Cina, *J. Phys. Chem. B* **110**, 18879 (2006).
- ⁴⁴P. F. Tekavec, T. R. Dyke, and A. H. Marcus, *J. Chem. Phys.* **125**, 194303 (2006).